A new dataset of river flood hazard maps for Europe and the Mediterranean Basin region

Francesco Dottori[1], Lorenzo Alfieri[2], Alessandra Bianchi[3], Jon Skoien[1], Peter Salamon[1]

1: European Commission, Joint Research Centre, Via E. Fermi 2749, 21027 Ispra, Italy.

2: CIMA Research Foundation, Savona, Italy

3: FINCONS SPA, Italy

Correspondence to: francesco.dottori@ec.europa.eu

Keywords: river flooding, flood hazard mapping, Europe, EFAS, Mediterranean Basin region.

Abstract

Continental scale hazard maps for riverine floods have grown in importance in the last years. Nowadays, they are used for a variety of research and commercial activities, such as evaluating present and future risk scenarios and adaptation strategies, as well as a support of national and local flood risk management plans. Here, we present a new set of high resolution (100m) hazard maps for river flooding that covers most of the geographical Europe and all the river basins entering the Mediterranean and Black Seas in the Caucasus, Middle East and Northern Africa countries. Maps represent inundation along 329'000 km of river network for six different flood return periods, expanding the previous datasets available in the region. The input river flow data is produced by the hydrological model LISFLOOD using new calibration and meteorological data, while inundation simulations are performed with the hydrodynamic model LISFLOOD-FP. In addition, we present a detailed validation exercise using official hazard maps for Hungary, Italy, Norway, Spain and the United Kingdom, that provides a more detailed evaluation of the new dataset in respect to previous works in the region. We find that modelled maps can identify on average two-thirds of reference flood extent, however they also overestimate flood-prone areas for flood probabilities below 1-in-100-year, while for return periods equal or above 500 years the maps can correctly identify more than half of flooded

29 areas. Further verification in North African and Eastern Mediterranean regions is needed to

30 better understand the performance of the flood maps in arid areas outside Europe. We attribute

31 the observed skill to a number of shortcomings of the modelling framework, such as the absence

32 of flood protections and rivers with upstream area below 500 km^2, and the limitations in

33 representing river channels and topography of low land areas. In addition, the different design

34 of reference maps (e.g. extent of areas included) affects the correct identification of the areas for

35 the validation, thus penalizing scores. However, modelled maps achieve comparable results to

36 existing large-scale flood models when using similar parameters for the validation. We

37 conclude that recently released high-resolution elevation datasets combined with reliable data of

38 river channel geometry may greatly contribute to improve future versions of continental-scale

39 flood hazard maps. The database is available for download at

40 http://data.europa.eu/89h/1d128b6c-a4ee-4858-9e34-6210707f3c81 (Dottori et al., 2020a).

41

1) Introduction

Nowadays, flood hazard maps are a basic component of any flood risk management strategy (EC 2007). They provide spatial information about a number of variables (such as flood extent, water depth, flow velocity) that are crucial to quantify flood impacts and therefore to evaluate flood risk. Moreover, they can be used as a powerful communication tool, allowing to quickly visualize the potential spatial impact of a river flood over an area.

Continental-scale and global-scale flood maps have grown in importance in the last years, and they are now used for a variety of research, humanitarian and commercial activities, and as a support of national and local flood management (Ward et al., 2015; Trigg et al., 2016). Global flood maps are used to provide flood risk information and support decision-making in spatial and infrastructure planning in countries where national level assessments are not available (Ward et al., 2015). Moreover, continental and global maps are vital for consistent quantification of flood risk and in projecting the impacts of climate change (Alfieri et al., 2015; Trigg et al., 2016; Dottori et al., 2018), allowing for comparisons between different regions, countries and river basins (Alfieri et al., 2016). Quantitative and comparable flood risk assessments are also necessary to derive measurable indicators of the targets set by international agreements such as the Sendai Framework for Disaster Risk Reduction (UNISDR, 2015).

In Europe, continental-scale flood hazard maps have been produced by Barredo et al. (2007), Feyen et al. (2012), Alfieri et al. (2014), Dottori et al. (2016a) and Paprotny et al. (2017). These maps have been used for a variety of studies, such as the evaluation of river flood risk under future socio-economic and climate scenarios (Barredo et al.,2007; Feyen et al., 2012; Alfieri et al., 2015), the evaluation of flood adaptation measures (Alfieri et al., 2016) and near-real time rapid risk assessment (Dottori et al., 2017).

The quality of continental-scale flood maps is constantly improving thanks to the increasing accuracy of datasets and modelling tools. Wing et al., (2017) developed a dataset of flood hazard maps for the conterminous United States using detailed national datasets and high-resolution hydrodynamic modelling, and demonstrated that continental-scale maps can achieve an accuracy similar to official national hazard maps, including maps based on accurate local-scale studies. Moreover, Wing et al. used the same official hazard maps to evaluate the performance of the global flood hazard model developed by Sampson et al. (2015). While the global model was less accurate than continental model, it could correctly identify over two-

thirds of flood extent. Conversely, European-scale maps have undergone limited testing against official hazard maps, due to limitations in accessing official data (Alfieri et al., 2014).

Here, we present a new set of flood hazard maps at 100m resolution (Dottori et al., 2020a), developed as a component of the Copernicus European Flood Awareness System (EFAS, www.efas.eu). The new dataset builds upon the map catalogue developed by Dottori et al (2016a) and feature different advances. The geographical extent of the new maps has been expanded to include all geographical Europe (with the exclusion of the Volga river basin), the rivers entering the Mediterranean Sea and the Black Sea (with the partial inclusion of the Nile river basin), plus Turkey, Syria and the Caucasus region. To our best knowledge these are the first flood hazard maps available at 100m resolution for the whole Mediterranean Basin region. The hydrological input is calculated using the latest version of the LISFLOOD hydrological model (van der Knijff et al., 2010; Burek et al, 2013; https://ec-jrc.github.io/lisflood/), based on updated calibration and meterological data in respect to the previous dataset by Dottori et al. (2016a). Flood simulations are performed with the hydrodynamic model LISFLOOD-FP (Bates et al., 2010; Shaw et al., 2021), following the approach developed by Alfieri et al., (2014; 2015).

To provide a comprehensive overview of the skill of the new maps, we perform a validation exercise using official hazard maps for a number of countries, regions and large river basins in Europe. The number and extent of the validation sites allows for a more detailed evaluation in respect to previous efforts by Alfieri et al. (2014) and Paprotny et al. (2017), even though none of the validation sites is located outside Europe due the unavailability of national flood maps. Moreover, we discuss the results of the validation in light of previous literature studies, we compare the performance of the present and previous version of the flood map dataset, and we discuss a number of tests with alternative datasets and methods.

2) Data and methods

In this Section we describe the procedure adopted to produce and validate the flood hazard maps. The hydrological input consists of daily river flow for the years 1990-2016. It was produced with the latest version of the hydrological model LISFLOOD (Section 2.1), based on interpolated daily meteorological observations. River flow data are analysed to derive frequency distributions, peak discharges and flood hydrographs, as described in Section 2.2. Flood

103 hydrographs are then used to simulate flooding processes at local scale with the LISFLOOD-FP
104 hydrodynamic model (Section 2.3). Finally, Section 2.4 describes the validation exercise and
105 the comparison of different approaches and input datasets.

2.1 The LISFLOOD model

107 LISFLOOD (Burek et al, 2013; van der Knijff et al., 2010) is a distributed, physically-based
108 rainfall-runoff model combined with a routing module for river channels. In this work we use
109 the latest updated version of LISFLOOD, released as open-source software and available at
110 https://ec-jrc.github.io/lisflood/. The model is applied to run a long-term hydrological
111 simulation for the period 1990-2016 at 5 km grid spacing and daily resolution, which provides
112 the hydrological input for the flood simulations. Note that the same simulation also provides
113 initial conditions for daily flood forecast issued by EFAS.

114 The long-term run of LISFLOOD is driven by gridded meteorological maps, derived by
115 interpolating meteorological observations from stations and precipitation datasets (see
116 Appendix A for details). The meteorological dataset has been updated in respect to the dataset
117 used by Dottori et al. (2016a) to include new stations and gridded datasets across the new EFAS
118 domain (Arnal et al. 2019). In addition, LISFLOOD simulations require a number of static input
119 maps such as land cover, digital elevation model, drainage network, soil parameters and
120 parameterization of reservoirs. All the static maps have been updated to cover the whole EFAS
121 domain depicted in Figure 1.

122 The current LISFLOOD version also benefits from an updated calibration at European scale,
123 based on the Evolutionary Algorithm approach (Hirpa et al., 2018) with the modified Kling-
124 Gupta efficiency criteria (KGE; Gupta et al., 2009) as objective function, and streamflow data
125 for 1990-2016 from more than 700 gauge stations. The results of the calibration and the
126 LISFLOOD hydrological skill are described in Arnal et al (2019), and summarized in the
127 Appendix B. We did not carry out a formal comparison with the previous LISFLOOD
128 calibration, which used a different algorithm and performance indicators (Zajac et al., 2013),
129 however the larger dataset of streamflow observations and the improvement of the calibration
130 routines should provide a better performance.

131 The geographical extent used in the present study to produce the flood maps follows the recent
132 enlargement of EFAS (Arnal et al., 2019), and it is shown in Figure 1. The new domain is

133 approximately 8'930'000 km² wide (an increase of 76% in respect with the previous extent). It

134 covers the entire geographical Europe (with the exclusion of the Volga river basin and a number

135 of river basins of the Arctic Sea in Russia), all the rivers entering the Mediterranean and Black

136 Seas (with a partial inclusion of the Nile river basin), plus the entire territories of Armenia,

137 Georgia, Turkey, and most of Syria and Azerbaijan. The river network included in the new

138 flood hazard maps has a total length of 329'000 km, with an 80% increase compared to the

139 previous flood maps (Alfieri et al., 2015; Dottori et al., 2016a).
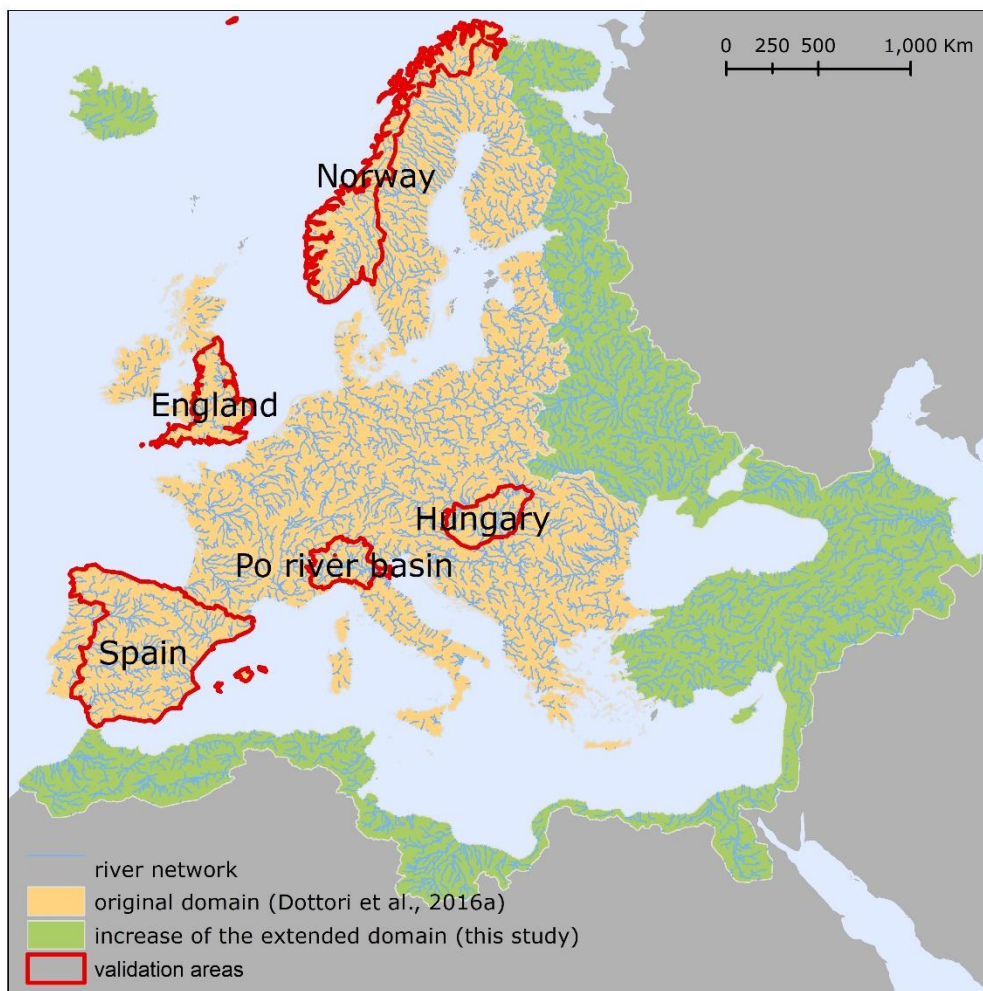
140

141 *Figure 1. Geographical extent of the EFAS extended domain covered by the present dataset of*

142 *flood hazard maps. The extent of the map dataset produced by Dottori et al. (2016a) is depicted*

143 *in beige, while the regions added with the extended domain are in green. The figure also*

144 *displays the river network considered by the flood maps and the areas used for the validation*

145 *exercise (see Sections 2.3 and 3).*

2.2 Hydrological input of flood simulations

The input hydrographs necessary for the flood simulations are derived from the LISFLOOD streamflow dataset described in Section 2.1, following the approach proposed by Alfieri et al. (2014). Streamflow data is available for the EFAS river network at 5 km grid spacing for rivers with upstream drainage areas larger than 500 km². For each pixel of the river network we selected annual maxima over the period 1990-2016 and we used the L-moments approach to fit a Gumbel distribution and calculate peak flow values for reference return periods of 10, 20, 50, 100, 200 and 500 years. Note that we also calculated the 30- and 1000-year return periods in limited parts of the model domain to allow validation against official hazard maps, see Section 2.3.

Subsequently, we calculate a Flow Duration Curve (FDC) from the long-term simulation. The FDC is obtained by sorting in decreasing order all the daily discharges, thus providing annual maximum values Q_D for any duration i between 1 and 365 days. Annual maximum values are then averaged over the entire period of data, and used to calculate the ratios ε_i between each average maximum discharge for i -th duration $Q_{D(i)}$ and the average annual peak flow (i.e. Q_D = 1 day). Design flood hydrographs are derived using daily time steps. The peak value is given by the peak discharge for the selected T- year return period Q_T, while the other values Q_i are derived multiplying Q_T by the ratio ε_i. The hydrograph peak Q_T is placed in the centre of the hydrograph, while the other values Q_i are sorted alternatively to produce a triangular hydrograph shape, as shown in Figure 2.
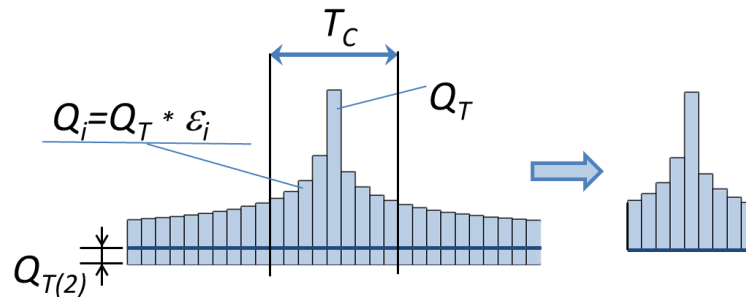
Figure 2. General scheme of flood hydrographs (adapted from Alfieri et al., 2014).

Because river channels are usually not represented in continental scale topography, flood hydrograph values are reduced by subtracting the 2-years discharge peak $Q_{T(2)}$, which is

commonly considered representative of river bank-full conditions. Note that the original DEM is not modified. The total duration of the hydrograph is given by the local value of the time of concentration T_c, therefore all the durations $> T_c$ are discarded from the final hydrograph.

2.3 Flood hazard mapping

The continental-scale flood hazard maps are derived from local flood simulations run all along the river network as in Alfieri et al. (2014). We use the DEM at 100 m resolution developed for the Catchment Characterization and Modelling Database (CCM; Vogt et al., 2007) to derive a high-resolution river network at the same resolution. Along this river network we identify reference sections every 5 km along stream-wise direction, and we link each section to the closest upstream section (pixel) of the EFAS 5km river network, using an partially automated procedure to ensure a correct linkage near confluences. In this way, the hydrological variables necessary to build the flood hydrographs can be transferred from the 5km to the 100m river network. Figure 3 describes how the 5km and 100m river sections are linked using a conceptual scheme.

Then, for every 100 m river section we run flood simulations using the 2D hydrodynamic model LISFLOOD-FP (Shaw et sl., 2021), to produce a local flood map for each of the six reference return periods. Simulations are based on the local inertia solver of LISFLOOD-FP developed by Bates et al. (2010), which is now available as open-source software (https://www.seamlesswave.com/LISFLOOD8.0). We use the CCM DEM as elevation data, the synthetic hydrographs described in Section 2.2 as hydrological input, and a mosaic of Corine Land Cover for the year 2016 (Copernicus LMS, 2017) and GlobCover for the year 2009 (Bontemps et al., 2009) to estimate the friction coefficient based on land use.

Finally, the flood maps with the same return period are merged together to obtain the continental-scale flood hazard maps. The 100m river network is included as a separate map in the dataset, to delineate which water courses have been considered in the creation of the flood hazard maps.
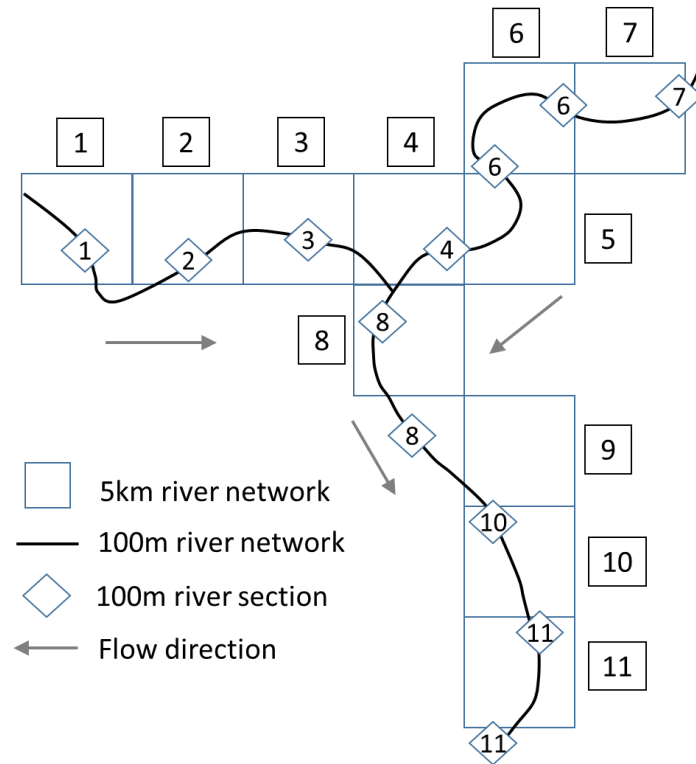
Figure 3. Conceptual scheme of the EFAS river network (5 km, squares) with the high-resolution network (100 m) and river sections (diamonds) where flood simulations are derived. The related sections of the two networks are indicated by the same number. Source: Dottori et al. (2017).

It is important to note that the flood maps developed do not take into account the influence of local flood defences, in particular dyke systems. Such limitation has been dictated mainly by the absence of consistent data at European scale. None of the available DEMs for Europe have the necessary accuracy and resolution to embed artificial embankments into elevation data. Moreover, there are no publicly available continental or national datasets describing the location and characteristics (e.g. dyke height, distance from river channel) of flood protections. Currently available datasets are based on the design return period of flood protection, e.g. the maximum return period of flood events that protections can withstand before being overflown, (Jongman et al., 2014; Scussolini et al., 2016). Most of the protection standards reported by these datasets for Europe are based on empirical regressions derived using proxy variables (e.g. gross domestic product, land use), with few data based on actual design standards. While these datasets have been applied to calculate flood risk scenarios (Alfieri et al., 2015) and flood

216 impacts (Dottori et al., 2017), they have important limitations when used for mapping flood
217 extent. Wing et al. (2017) linked the flood return period of protection standards with flood
218 frequency analysis to adjust the bank height of the river channels, however with impaired
219 performance of the model. Moreover, recent studies for United States suggest that empirical
220 regressions based on gross domestic product and land use may not be reliable (Wing et al.,
221 2019).

222 Despite these limitations, maps not accounting for physical flood defences may be applied to
223 estimate the flood hazard in case of failure of the protection structures, and for flood events
224 exceeding protections levels.

225 *2.3 Validation of flood hazard maps*

226 *2.3.1 Selection of validation areas and maps*

227 The validation of large-scale flood hazard maps requires the use of benchmarks with one or
228 more datasets with extension and accuracy commensurate to the modelled maps. For instance
229 Wing et al. (2017) used the official hazard maps developed for the conterminous United States
230 to evaluate the performance of two flood hazard models, respectively designed to produce
231 global-scale and continental-scale flood maps (see Introduction). In Europe, all member states
232 of the European Union as well as the United Kingdom have developed national datasets of
233 flood hazard maps for a range of flood probabilities (usually expressed with the flood return
234 period), following the guidelines of the EU Floods Directive (EC 2007). While these maps are
235 generally available online for consultation on Web-GIS services, only few countries and river
236 basin authorities make the maps available for download in a format that allows comparison with
237 geospatial data. Table 1 presents the list of flood hazard maps that could be retrieved and used
238 for the validation exercise, while Figure 1 shows their geographical distribution. Note that the
239 relevant links to access these maps are provided in the Data Availability section.

240 Even though more official maps are likely to become available in the near future, the maps here
241 considered offer an acceptable overview of the different climatic zones and floodplain
242 characteristics of the European continent. Conversely, we could not retrieve national or regional
243 flood hazard maps outside Europe, meaning the skill of the modelled maps could not be tested
244 in the arid regions in Northern Africa and Eastern Mediterranean. In Norway, Spain, the United

245 Kingdom and the Po River Basin the official maps take into account flood defences, which are

246 instead not represented in the modelling framework. Official maps for England also include

247 areas prone to coastal flooding events (such as tidal and storm surges). None of the official

248 maps include areas prone to pluvial flooding, which are therefore not considered in this

249 analysis.

250 For the comparison exercise, we selected available maps for return periods for which flood

251 extent is likely to be less conditioned by flood defences. For instance, the main stem of the Po

252 river is protected against the 1-in-200-year flood events (Wing et al., 2019), whereas protection

253 standards in England and Norway are usually above 20 years (Scussolini et al., 2016).

254 Conversely, we consider the 1-in-30-year map for Hungary and the 1-in-10-year map for Spain

255 because flood defences are either not accounted for (Hungary) or their extent and design level is

256 not known (Spain).

257

Country	Geographical extent	Return periods used	Defences included
Hungary	Country scale	30 – 100 - 1000 years	No
Italy	Po River Basin	500 years	Yes
Norway	Country scale	100 years	Yes
Spain	Country scale	10 -100 - 500 years	Yes
United Kingdom	England	100 - 1000 years	Yes

258 *Table 1. List and characteristics of the flood hazard maps used in the validation exercise. The*

259 *links for dowloading the maps are provided in the Data Availability section.*

2.3.2 Performance metrics and validation procedure

261 The national flood hazard maps listed in Table 1 are provided as polygons of flood extent, with

262 no information on water depth nor on original resolution of data. According to Sampson et al.

263 (2015), the official flood hazard maps for England are constructed using DEMs of at least 5 m

resolution, therefore flood extent maps should be of comparable resolution. Reference flood maps for the Po basin and Spain are likely to have a similar resolution since they are based on LIDAR elevation data (MITECO 2011). For the comparison, official reference maps have been converted to raster format with the same resolution as the modelled maps (i.e. 100m), while the latter have been converted to binary flood extent maps. To improve the comparison between modelled and reference maps we applied a number of corrections. First, we used the CORINE Land Cover map to exclude permanent water bodies (river beds of large rivers or estuaries, lakes, reservoirs, coastal lagoons) from the comparison. Second, we restricted the comparison area around modelled maps to exclude the elements of river network (e.g. minor tributaries) included in the reference maps but not in the modelled maps. We used a different buffer extent according to each study area, considering the floodplain morphology and the variable extent and density of mapped river network. For instance, in Hungary we applied a 10-km buffer around modelled maps to include the large flooded areas reported in reference maps and avoid overfitting. In England, we used a 5-km buffer due to the high density of the river network mapped in the official maps; the buffer is also applied to mask out coastal areas far from rivers estuaries, because official maps include flood-prone areas due to 1-in-200-year coastal flood events. We calculated that flood-prone areas inside the 5km buffer correspond to 73% of the total extent for the 1-in-100-year flood. For the Po river Basin, we excluded from the comparison the areas belonging to the Adige River Basin and the lowland drainage network, which are not included in the official hazard maps. In Spain and Norway official flood hazard maps have only been produced where relevant assets are at risk, according to available documentation [MITECO 2011; NVE 2020]. We therefore restricted the comparison only to areas where official flood hazard maps have been produced. Table 2 provide the list of parameters used to determine the areas used for the comparison.

Test area	Buffer value (reference maps)	Buffer value (modelled maps)
Hungary	NA	10 km
Po River Basin	NA	See main text
Norway	5 km	5 km

| Spain | 5 km | 5 km |
| England | NA | 5 km |

Table 2. List of parameters used to determine the extent of areas used for comparing reference and modelled maps (NA: buffer not applied).

We evaluate the performance of simulated flood maps against reference maps using a number of indices proposed in literature (Bates and De Roo, 2000; Alfieri et al., 2014; Dottori et al., 2016b; Wing et al., 2017). The hit ratio HR evaluates the agreement of simulated maps with observations and it is defined as:

$$HR = (Fm \cap Fo)/(Fo) \times 100 \qquad (1)$$

where $Fm \cap Fo$ is the area correctly predicted as flooded by the model, and Fo indicates the total observed flooded area. HR scores range from 0 to 1, with a score of 1 indicating that all wet cells in the benchmark data are wet in the model data. The formulation of the hit ratio does not penalize overprediction, which can be instead quantified using the false alarm ratio FAR:

$$FAR = (Fm/Fo)/(Fm) \times 100 \qquad (2)$$

where Fm/Fo is the area wrongly predicted as flooded by the model. FAR scores range from 0 (no false alarms) to 1 (all false alarms). Finally, a more comprehensive measure of the agreement between simulations and observations is given by the critical success index CSI, defined as:

$$CSI = (Fm \cap Fo)/(Fm \cup Fo) \times 100 \qquad (3)$$

where $Fm \cup Fo$ is the union of observed and simulated flooded areas. CSI scores range from 0 (no match between model and benchmark) to 1 (perfect match between benchmark and model).

2.4 Additional tests

To choose the best possible methodologies and datasets to construct the flood hazard maps, we have performed a number of tests using recent input datasets as well as by alternative strategies to account for vegetation effects on elevation data.

2.4.1 Elevation data

It is well recognized that the quality of flood hazard maps strongly depend on the accuracy of elevation data used for modelling (Yamazaki et al., 2017). This is especially crucial for continental scale maps, since the quality of available elevation datasets is rarely commensurate to the accuracy required for modelling flood processes [Wing et al., 2017]. Moreover, high-resolution and accurate elevation data such as LIDAR-based DEMs cannot be used for reasons of consistency, given that these data are only available for few areas and countries.

The recent release of new global elevation models have the potential for improving the accuracy of large scale flood simulations, and hence the quality of flood hazard maps. Here, we test the use of the MERIT DEM (Yamazaki et al., 2017) within the proposed modelling approach and we compare the results with those obtained with CCM DEM. The MERIT DEM is based on the SRTM data, similarly to CCM DEM, however it has been extensively corrected and improved through comparisons from other large scale datasets, to eliminate error biases, to improve data accuracy at high latitudes (areas above 60° are not covered by SRTM) and compensate for factors like vegetation cover. Note that areas above 60° in CCM DEM were derived from national datasets, and therefore it is where the two datasets are likely to differ most.

2.4.2 Correction of elevation data with land use

The CCM DEM elevation dataset is mostly based on SRTM data and therefore elevation data can be spuriously increased by the effect of vegetation canopy in densely vegetated areas, and by buildings in urban areas. Recent research works proposed advanced techniques to remove surface artefacts, based on artificial neural networks (Wendi et al., 2016, Kulp and Strauss, 2018) or other machine learning methods (Liu et al., 2018; Meadows and Wilson, 2021). Most approaches correct DEM elevation with higher-accuracy datasets, using auxiliary data such as tree density and height for correcting vegetation bias (as done for the MERIT-DEM by Yamazaki et al., 2017), whereas elevation bias in urban areas can be corrected using night light, population density, or Open Street Map elevation data (Liu et al., 2018). Given that improving elevation data is not the main scope of this work, we opted for applying a simpler method for quickly correcting the CCM DEM elevation data. Specifically, we use the land cover map derived from Corine Land Cover and GlobCover to identify densely vegetated areas and urban areas, and we applied a correction factor as a function of local land use to locally reduce

344 elevation. The correction factor varies from 8m for dense forested areas, to 2m for urban areas.
345 Note that this values are based on the findings of previous literature studies such as Baugh et al.
346 (2013) and Dottori et al. (2016b), while a formal calibration was not undertaken.

3) Results and discussion

348 We present the outcomes of the validation exercise by describing first the general results at
349 country and regional scale in Section 3.1. Then, we discuss in the main text the outcomes for
350 England, Hungary and Spain (Section 3.2), while the Norway and Po river basin case studies are
351 presented in the Appendix C. We also complement the analysis with additional validation over
352 major river basins in England and Spain. In Section 3.3 we compare our results with the
353 validation exercise carried out by Wing et al. (2017) and with the findings of other literature
354 studies. Finally, in Section 3.4 and 3.5 and Appendix B we compare the performance of the
355 present and previous version of the flood map dataset, and we discuss the results of the tests
356 with different elevation data and strategies to account for vegetation.

3.1 Validation of modelled maps at national and regional scale

358 Table 3 presents the results of the validation for each testing area and return period. The
359 performance metrics are calculated using the total extent of the reference and modelled maps
360 with the same return period. The first visible outcome is the low scores for the comparisons
361 with reference maps with high probability of flooding, i.e. low flood return periods (<30 years).
362 Performances improve markedly with the increasing of return periods due to the decrease of
363 false alarm rate FAR, while the hit rate HR does not vary significantly. In particular, critical
364 success index (CSI) values approach 0.5 for the low probability flood maps, i.e., for return
365 periods equal or above 500 years. Considering that most of the reference flood maps include the
366 effect of flood defences (contrary to the modelled maps), these results suggest that the majority
367 of rivers in the study areas may be protected for flood return periods around 100 years or lower,
368 as indeed reported by available flood defence databases (Scussolini et al., 2016). Differences
369 between simulated and reference hydrological input are likely to influence the skill of modelled
370 flood maps. However, further analyses are difficult because we have no specific information on
371 the hydrological input used for the reference flood maps (e.g. peak flows, hydrograph shape). In
372 the following sections, we use the skill of the LISFLOOD long-term simulation to evaluate the

agreement between modelled and observed hydrological regime, but this does not necessarily translate to extreme values. High-probability floods are also sensitive to the method used to reproduce river channels, and the simplified approach used in this study might underestimate the conveyance capacity of channels (see Section 3.2.2 for an example). Finally, the better performance for low-probability floods may also depend on floodplain morphology, where valley sides create a morphological limit to flood extent.

	RP	**HR**	**FAR**	**CSI**
Spain	10	0.58	0.65	0.28
Hungary	30	0.77	0.88	0.11
Spain	100	0.63	0.44	0.42
Hungary	100	0.76	0.74	0.24
Norway	100	0.70	0.72	0.25
England	100	0.53	0.31	0.43
Po River Basin	500	0.60	0.13	0.56
Spain	500	0.61	0.36	0.45
Hungary	1000	0.76	0.45	0.47
England	1000	0.52	0.12	0.48

Table 3. Results of the validation against official flood hazard maps: value of the performance indices at country and regional scale. RP=Return Period, HR=Hit Ratio, FAR= False Alarm Ratio, CSI=Critical Success Index.

3.2 Discussion of results at national and regional scale

The results in Table 3 highlight considerable differences in the skill of the flood maps across countries and regions. While some differences may arise from the variability of floodplain morphology and model input data, others are attributable to the different methods applied to produce the reference maps (MITECO 2011; NVE 2020). In the following sections we examine in more detail the outcomes for each study area.

3.2.1 England

According to Table 3, modelled flood maps tend to underestimate flood extent in England, as visible by the hit rate values around 0.5 (e.g. out of every two flooded cells, only one is correctly identified as flooded by the model). Such result is confirmed when focusing the analysis on the major river basins of England, as reported in Table 4. Notably, HR has generally marginal or no increases with the increase of return period considered, while FAR values have a marked decrease. The results of reported by Arnal et al. (2019) and summarized in Figure B1 suggest a fair hydrological skill of the LISFLOOD calibration in England, with KGE values generally above 0.5. However, there is not a clear correlation between hydrological and flood map skill, with some basins (e.g. Thames) showing high KGE values but relatively low CSI values.

For the Thames basin, the low CSI value is likely influenced by the tidal flooding component from London eastwards. According to Sampson et al. (2015), the official flood hazard map assumes a 1 in 200 year coastal flood along with failure of the Thames tidal barrier, whereas our river flood simulations use the mean sea level as boundary condition and do include storm surge and tidal flooding. Concurrent fluvial-tidal flooding processes occur in other river estuaries, so this might reduce the skill of the modelled maps. Furthermore, the Thames catchment is heavily urbanized and has extensive flood defense and alleviation schemes compared the other catchments (Sampson et al., 2015). Both aspects might increase the elevation bias of CCM DEM and complicate the correct simulation of extreme flood events.

Catchments	100-year RP			1000-year RP		
	HR	**FAR**	**CSI**	**HR**	**FAR**	**CSI**
England	**0.53**	**0.31**	**0.43**	**0.52**	**0.12**	**0.48**
Ouse	0.57	0.39	0.42	0.56	0.19	0.49
Severn	0.64	0.24	0.53	0.63	0.20	0.54
Thames, above Lea	0.56	0.46	0.38	0.55	0.23	0.47
Trent	0.63	0.28	0.50	0.59	0.06	0.57
Tyne	0.51	0.43	0.37	0.52	0.28	0.43

Table 4. Validation indices in England and in major river basins.

413   Besides these results, the visual inspection of reference maps suggest that the underestimation is

414   partly caused by the high density of mapped river network in the reference maps, in respect to

415   modelled maps. Indeed, the modelling framework excludes river basins with an upstream basin

416   area below 500 km^2, meaning that EFAS maps only cover main river stems but miss out several

417   smaller tributaries. This is clearly visible over the Severn and in the upper Thames basins

418   (Figure 4), and might also explain the lower skill in the lowlands of Ouse and Trent rivers,

419   where the contributions of main river stems and tributaries to the flood extent are difficult to

420   separate. Including minor tributaries in the flood maps would require either to increase the

421   resolution of the climatological forcing to reproduce intense local rainfall, or to add a pluvial

422   flooding component as done by Wing et al. (2017). Finally, areas prone to storm surge and tidal

423   flooding around river estuaries might further reduce the overall skill of modelled maps, despite

424   the 5km buffer applied.
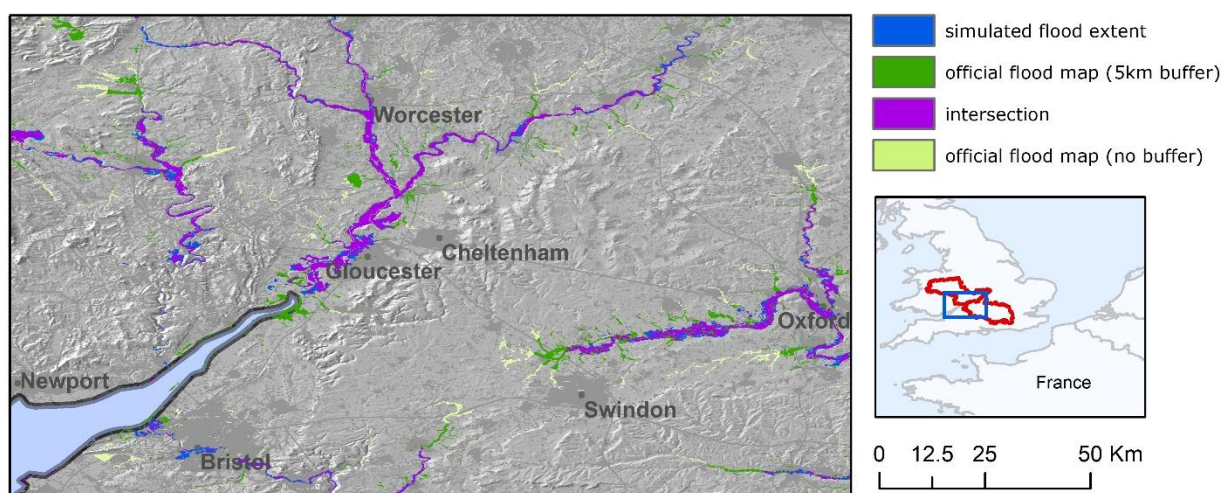
425

426   *Figure 4. Comparison of modelled (blue) and reference (green) flood hazard maps (1-in-100-*

427   *year) over the Severn (centre) and in the upper Thames basins in England (on the right). Purple*

428   *areas denotes intersection (agreement) between the modelled and reference set of maps. The*

429   *original reference maps (i.e. with no masking around modelled maps) are shown in light green.*

430

431   *3.2.2 Hungary*

432   The results in Table 3 for Hungary show a general tendency to overestimate flood extent for all

433   return periods. HR values are consistently high and do not change much with the return period.

Conversely, FAR is very high for the 1-in-30 year flood map and still considerable even for the 1-in-1000 year flood map. Arnal et al (2019) reported a fair hydrological skill of LISFLOOD (KGE values >0.5) for the calibration period, even though KGE validation values were considerably low for the Tisza River.

Given that flood defences are not modelled in reference maps, the observed results may be explained by assuming a large conveyance capacity of river channels. For instance, the 1-in-100 year reference map show relatively few flooded areas for the Danube main stem (Figure 5), thus suggesting that the main channels can convey the 1-in-100-year discharge without overflowing. Conversely, river channels in the modelling framework are assumed to convey only the 1-in-2-year discharge. Obviously, the same considerations can be made for 1-in-30-year discharge for the majority of river network, which explains the very low scores. Furthermore, artificial structures such as road embankments and drainage network may further reduce flood extent in lowland areas, leading to further overestimation given the fact that these features are not represented in the DEM. These findings highlight the need for high-resolution DEM fed with local-scale information to achieve adequate performance in lowland areas, as observed also by Wing et al (2019b).
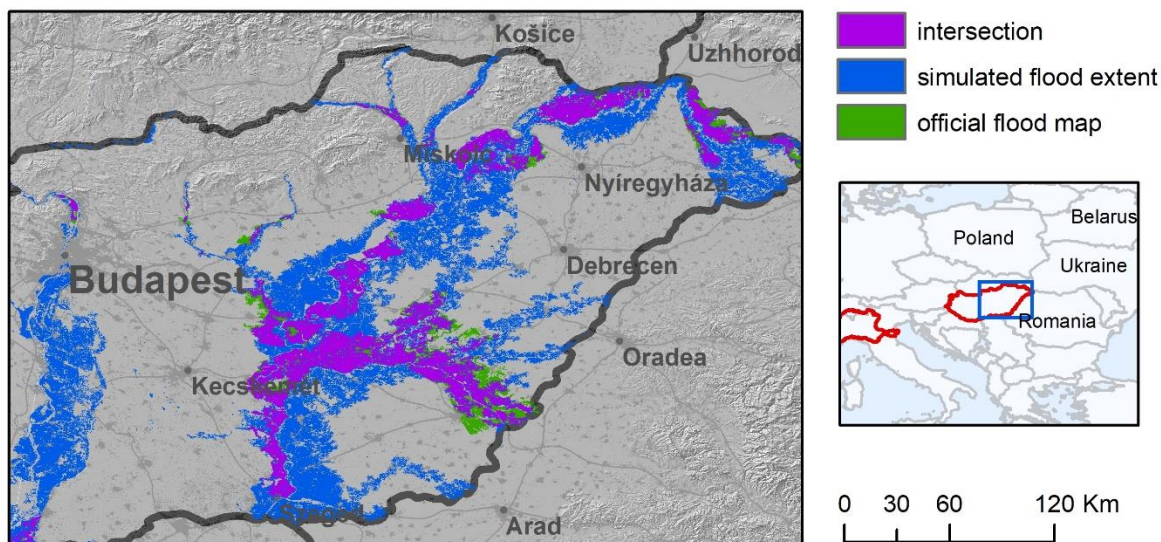
Figure 5. Comparison of modelled (blue) and reference (green) flood hazard maps (1-in-100-year) over the Danube (left) and Tisza (right) rivers in Hungary. Purple areas denotes the intersection between the modelled and reference set of maps.

3.2.3 Spain

The performance of the modelled maps in Spain show a fairly stable HR value and decreasing FAR values with increasing return periods, similarly to what was observed for England and Hungary. The analysis of the results for the major river basins of the Iberian Peninsula, reported in Table 5, provide further insight on the skill of flood maps. A number of basins exhibit both large HR and FAR such as the Duero, Tajo and Guadalquivir basins. Rivers in South-East Spain (Segura, Jucar) have relatively low HR values, while the modelled maps perform better in the Ebro river basin. The interpretation of results requires to consider different aspects. The poor results for the 1-in-10-year maps are likely due to the effect of flood protection structures, such as dykes and flood regulation systems, which are probably relevant also for the 1-in-100-year map. Indeed, most Iberian rivers are regulated by multiple reservoirs, which are often used to reduce flood peaks according to specific operating rules. While dykes are not represented in the inundation model, reservoirs are included in the LISFLOOD model through a simplified approach, given that operating rules are not known. As such, the real and modelled hydrological regimes might differ significantly, including flow peaks of low-probability flood events. This is reflected also by the low hydrological skill of LISFLOOD, with KGE values generally below 0.5 with few exceptions (Figure B1).

In addition, the comparison of modelled and reference maps is affected by the partial coverage of the reference inundation maps in several river basins. According to the information available in the official website (MITECO 2011) large sections of the river network in the basins of the Duero, Tajo, Guadiana and Guadalquivir rivers have not been analyzed, due to the absence of relevant assets or inhabited places at risk. Even though this has been accounted by restricting the area of comparison around reference maps, a visual inspection of the maps being compared shows spurious overestimation around the edges of reference map polygons (Figure 6). Finally, the low HR values scored in rivers in South-East Spain (Segura, Jucar) are partially explained by the presence of several tributaries not included in EFAS maps.

Catchments	10-year RP			100-year RP			500-year RP		
	HR	**FAR**	**CSI**	**HR**	**FAR**	**CSI**	**HR**	**FAR**	**CSI**
Spain	**0.58**	**0.65**	**0.28**	**0.63**	**0.44**	**0.42**	**0.61**	**0.36**	**0.45**
Duero	0.60	0.74	0.22	0.65	0.55	0.36	0.65	0.46	0.42
Ebro	0.71	0.46	0.45	0.75	0.27	0.59	0.74	0.23	0.61
Guadalquivir	0.67	0.66	0.29	0.69	0.49	0.42	0.66	0.46	0.42
Guadiana	0.52	0.63	0.28	0.60	0.42	0.42	0.61	0.31	0.48
Jucar	0.32	0.89	0.09	0.53	0.46	0.36	0.51	0.39	0.39
Tajo	0.60	0.85	0.14	0.70	0.63	0.32	0.69	0.49	0.41
Segura	0.18	0.89	0.07	0.38	0.52	0.27	0.41	0.24	0.36

486   *Table 5. Validation indices in Spain and in some test river basins.*
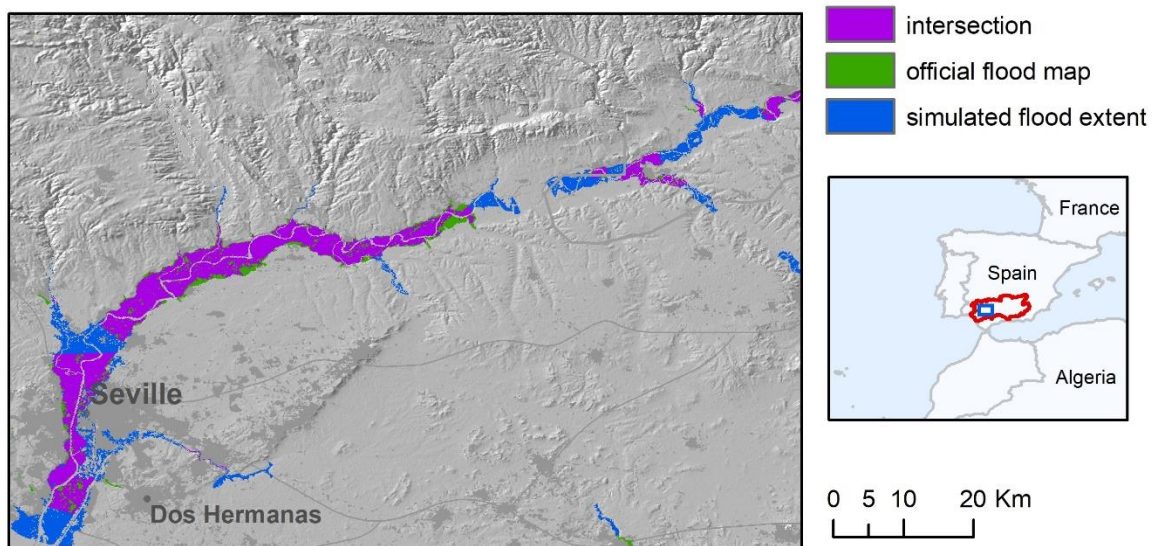
487

488   *Figure 6. Comparison of modelled (blue) and reference (green) flood hazard maps (1-in-100-*

489   *year) over a stretch of the Guadalquivir river basin, Spain. Purple areas denote the intersection*

490   *between the two set of maps.*

491   ### *3.3 Comparison with previous continental-scale validation studies*

492   To put the described outcomes in context, we compare them with the validation exercises

493   performed by Sampson et al. (2015) over the Thames and Severn rivers in England, and by

494   Wing et al. (2017) over United States. The study by Wing et al. is, to our knowledge, the first

495   study that carried out a consistent validation of modelled flood hazard maps at continental scale.

496   Bates et al. (2021) have recently updated the work by Wing et al. by including pluvial and

497   coastal flooding components in the modelling framework, but their work is not considered here.

498   A comparison of validation metrics of the three studies are shown in Table 6 and 7. For our

499   framework, we calculated each index in Table 6 using the overall modelled and reference flood

500   extent available for each return period (e.g. the value for the 100-year maps includes reference

501   and modelled maps for England, Spain and Norway). As such, each area is weighted according

502   to the extent of the corresponding flood map.

503   As can be seen in Table 6, the continental-scale model by Wing et al. achieved the highest

504   scores both for 100y and 500y return periods. However, this model is based on national datasets

505   with higher accuracy and resolution than those available for the European continent (e.g. a 10m-

506   resolution DEM and a detailed catalogue of flood defences). The global and European models

507   have comparable hit rates for the 100-year flood maps (0.68 and 0.65 respectively), but the

508   former exhibits a much lower FAR value (0.34 compared to 0.61 of the European model), and a

509   higher HR value for the 500-year maps.

510   The higher HR values scored by the US and global models might depend on the higher density

511   of the modelled river network, which includes river reaches up to 50km^2 by simulating both

512   pluvial and fluvial flooding processes. The lower FAR values of the US and global models

513   might be explained by the inclusion of flood defences. In the US model, defences are explicitly

514   modelled using the US dataset of flood defences, while the global model parameterizes flood

515   defences through the adjustment of channel conveyance using socioeconomic factors and degree

516   of urbanization (Wing et al., 2017). However, Wing et al observed that the latter methodology

517   had a negligible effect on hit rates in defended areas, when compared against an undefended

518   version of the model.

519   Another possible reason for the low FAR values is the different approach used in the validation

520   method. Wing et al. applied a narrow 1km buffer around official maps to constrain the area of

521   comparison and avoid spurious over-prediction in areas not considered by official maps.

522   However, this might result in a reduction of true false alarms, because part of overestimated

523   flood areas can go undetected. To verify this hypothesis, we recalculated the performance

524   indices against the 100-year reference map in Spain using a 1km buffer instead of the 5km

525   previously applied to constrain the validation area. As a result the false alarm ratio dropped

526   from 0.44 to 0.34, similar to the performance of the global model. However, we observed a

527   reduction of true false alarms, especially in river basins with continuous map coverage such as

528   the Ebro, Jucar and Segura.

529

	RP	HR	FAR	CSI
US model (Wing et al.)	100	0.82	0.37	0.55
Global model (Wing et al.)	100	0.69	0.34	0.50
European model (this study)	100	0.66	0.61	0.32
US model (Wing et al.)	500	0.86	na	na
Global model (Wing et al.)	500	0.74	na	na
European model (this study)	500	0.61	0.24	0.51
European model (this study)	1000	0.68	0.39	0.47

530   *Table 6. Comparison of the performance metrics for the European model described in the*

531   *present study and the two models evaluated in the study by Wing et al. (2017).*

532

533   The comparison of HR, FAR and CSI values show better scores for the global maps by

534   Sampson et al. (2015) in respect to our modelled maps (Table 7).

535

	HR	FAR	CSI
Thames (this study)	0.56	0.46	0.38
Thames (Sampson et al. 2015)	0.73	0.3	0.56
Severn (this study)	0.64	0.24	0.53
Severn (Sampson et al. 2015)	0.83	0.23	0.67

536   *Table 7. Comparison of the performance metrics for the maps described in the present study*

537   *and the global maps by Sampson et al. (2015). Metrics for the latter study are calculated*

538   *removing all channels with upstream areas of less than 500 km2.*

539

540   The different masking applied to reference flood maps may explain some of the differences:

541   Sampson et al. removed all channels with upstream areas of less than 500 km^2, whereas here we

542   use a simpler 5km buffer around modelled maps. The exclusion of permanent river channels in

543   our comparison may further penalize the overall score especially for the Thames, which as a

544   rather large channel estuary. Besides these differences in the validation, the better metrics of the

maps by Sampson et al. may depend on a more accurate hydrological input (based on regionalization of gauge station data) and a better correction of urban elevation bias (based on a moving window filter instead of the constant correction values applied here).

To provide further context, the US model by Wing et al. (2017) attained average CSIs of ~0.75 against a number of detailed local models, whereas flood models built and calibrated for local applications may achieve CSI scores up to 0.9 when benchmarked against very high quality data (see Wing et al., 2019a). Fleischmann et al. (2019) recently proposed that regional-scale models can provide locally relevant estimates of flood extent when CSI > 0.65. Although the overall values shown in Table 3 are consistently below this threshold, better results are observed for a number of river basins, as shown in Tables 4 and 5.

3.4 Comparison with the previous flood map dataset

Table 7 compares the performances of the flood hazard maps described in the present study (version 2) with the previous version developed by Dottori et al. (2016a; version 1). The comparison is shown for England and Hungary. Results for all other areas are comprised within the range of results shown in Table 3. As can be seen, differences are generally reduced across the different areas and return periods. Version 1 of the flood maps produced slightly better results in Hungary for the 100- and 1000-year return period (increased CSI and HR, lower FAR), while version 2 has somewhat improved performances in England, mainly driven by higher HR.

	RP (y)	F2/F1	ΔHR	ΔFAR	ΔCSI
Hungary	30	0.97	-0.5%	-0.4%	2.9%
Hungary	100	1.00	-2.1%	0.7%	-2.4%
Hungary	1000	1.01	-3.6%	5.7%	-6.3%
England	100	1.05	9.4%	1.7%	7.3%
England	1000	1.04	8.2%	-1.1%	7.7%

Table 7. Comparison of performances of the flood hazard maps described in the present study and developed by Dottori et al. (2016a). Table reports the ratio between flood extents (F2/F1) and the difference between version 2 and 1 of the HR,CSI,FAR values.

569   These outcomes may be interpreted considering the changes in input data between the two
570   versions, and the structure of the modelling approach and of input data, which in turn has not
571   changed substantially. The main difference between the two map versions is given by the
572   hydrological input, with version 2 using the latest calibrated version of the LISFLOOD model.
573   For the 100-year return period, peak flow values of version 2 are on average 35% lower than
574   version 1 in Hungary, and 16% lower in England. However, similar decreases are also observed
575   for the 1-in-2-year peak discharge which determines bankful discharge. The resulting reduction
576   in channel hydraulic conveyance in respect to version 1 is likely to offset the decrease of peak
577   flood volumes, which explain the small difference in overall flood extent given by the F2/F1
578   parameter in table 7. Such result confirm that the knowledge of river channel geometry is
579   crucial to correctly model the actual channel conveyance and thus improve inundation
580   modelling. Other differences in input data are given by minor changes in Manning's parameters
581   and in the EFAS river network, which might contribute to the observed differences.
582

583   ## 3.5 Influence of elevation data

584   Table 8 compares the metrics calculated with CCM DEM elevation data against the same
585   metrics for the modelled flood maps based on MERIT-DEM. The comparison is carried out for
586   England, Hungary and the Po river basin. Performance is slightly improved by the use of
587   MERIT-DEM data for all areas and return periods, in particular through the reduction of FAR,
588   even though the overall increase of CSI values is limited to few percentage points.
589

	RP (y)	ΔF	ΔHR	ΔFAR	ΔCSI
Hungary	100	-5.3%	0.0%	-2.0%	5.1%
Hungary	1000	-5.9%	-0.1%	-7.6%	5.2%
England	100	0.0%	2.6%	-5.7%	3.8%
England	1000	1.7%	2.8%	-7.8%	3.2%
Po	500	0.2%	0.9%	-4.3%	3.4%

590   *Table 8. Comparison of performances of the flood hazard maps described in the present study*
591   *and developed by Dottori et al. (2016a based on the MERIT-DEM (a) and CCM-DEM (b).*

592 *Table reports the ratio between flood extents F and the differences for HR,CSI,FAR (e.g. (HRa-*
593 *HRb)/HRa).*

594

595 Because of this limited improvement and the considerable amount of time required to rerun the
596 complete set of flood hazard maps (several days for each return period) it was decided not to
597 update the flood maps using the MERIT-DEM as elevation data. Moreover, new high-resolution
598 datasets such as the Copernicus DEM (ESA-Airbus 2019), the 90m version of TanDEM-X
599 dataset (https://geoservice.dlr.de/web/dataguide/tdm90), and MERIT-HYDRO (Yamazaki et
600 al., 2019) have recently become available, and therefore future research could focus on
601 performing additional comparisons to identify which dataset is most suitable for inundation
602 modelling in Europe.

603

604 ## 4) Conclusions and ongoing work

605 We presented here a new dataset of flood hazard maps covering the geographical Europe and
606 including large parts of the Middle East and river basins entering the Mediterranean Sea. This
607 dataset significantly expands the previous available flood maps datasets at continental scale
608 (Alfieri et al., 2014; Dottori et al., 2016a), and therefore constitutes a valuable source of
609 information for future research studies and flood management, especially for countries where no
610 official flood hazard maps are available. The new maps also benefit of updated models and new
611 calibration and meteorological data. The maps are being used for a range of applications at
612 continental scale, from evaluating present and future river flood risk scenarios, to the cost-
613 benefit assessment of different adaptation strategies to reduce flood impacts, and for
614 comparisons between different regions, countries and river basins (Dottori et al, 2020b).
615 Moreover, the flood hazard maps are designed to be integrated with the European Flood
616 Awareness System (EFAS), and will be used to perform operational flood impact forecasting in
617 EFAS (Dottori et al., 2017).
618 We performed a detailed validation of the modelled flood maps in several European countries
619 against official flood hazard maps. The resulting validation exercise is the most complete
620 undertaken so far for Europe to our best knowledge, and provided a comprehensive overview of
621 the strengths and limitations of the new maps. Nevertheless, the unavailability of reference

622   flood maps outside Europe did not allow any validation in the arid regions in North Africa and
623   Eastern Mediterranean. In these areas, further research will be needed to better understand the
624   performance of the flood mapping procedure here proposed. Modelled maps generally achieve
625   low scores for high and medium probability of flooding. For the 1-in-100-year flood
626   probability, the modelled maps can identify on average two-thirds of reference flood extent,
627   however they also largely overestimate flood-prone areas in many regions, thus hampering the
628   overall performance. Performances improves markedly with the increasing of return period,
629   mostly due to the decrease of the false alarm rates. In particular, critical success index (CSI)
630   values approach and in some cases exceed 0.5 for return periods equal or above 500 years,
631   meaning that the maps can correctly identify more than half of flooded areas in the main river
632   stems and tributaries of different river basins.

633   It is important to note that the validation was affected by problems in identifying the correct
634   areas for a fair comparison, because of the different density of the mapped river network in
635   reference and modelled maps. In our study we opted for a conservative approach using large
636   buffers to constrain comparison areas, which possibly penalized the model performance, e.g.
637   due to spurious false alarms in areas not considered by official maps. However, we observed
638   that the proposed maps achieve comparable results to other large-scale flood models when using
639   similar parameters for the validation.

640   The low skill of modelled maps for high and medium probability of flooding, with large
641   overestimations observed in different lowland areas, is mostly motivated by the non-inclusion
642   of flood defences in the modelling framework and the simplified representation of channel
643   hydraulic conveyance, due to the absence of datasets at European scale describing river
644   channels and defence structures (i.e. design standards and location of dyke systems). Such
645   information combined with high-resolution DEM fed with local-scale information (artificial and
646   defence structures) is crucial to improve the performance of large-scale flood models and apply
647   more realistic flood modelling tools, as observed also by Wing et al (2017, 2019b). On this
648   point, we found that the modelling approach has limited sensitivity to changes in the
649   hydrological input, because channel conveyance is linked to streamflow characteristics. Such
650   finding highlight the need for independent data of river channel width, shape and depth to better
651   reproduce streamflow and flooding processes. Moreover, the improved results offered by the
652   use of the MERIT-DEM elevation data suggest that recent high-resolution datasets such as the

653 Copernicus   DEM   (ESA-Airbus   2019),   TanDEM-X

654 (https://geoservice.dlr.de/web/dataguide/tdm90), and MERIT-HYDRO (Yamazaki et al., 2019)

655 may offer a viable solution to improve future versions of continental-scale flood hazard maps in

656 Europe.

657 Increasing map coverage by including the minor river network is likely to improve the skill of

658 modelled maps. However, this might require the use of a different modelling approach to

659 account for pluvial flooding (Wing et al., 2017; Bates et al., 2021), along with reliable model

660 climatology to represent small-scale precipitation processes. Improving the simulation of

661 reservoirs may also reduce the difference between the real and modelled hydrological regimes

662 in regions such as the Iberian Peninsula and the Alps.

663 ## *Data availability*

664 The dataset described in this manuscript is accessible as part of the data collection "Flood

665 Hazard Maps at European and Global Scale" at the JRC data Catalogue

666 (https://data.jrc.ec.europa.eu/collection/floods/).

667 Please refer to the dataset as follows: Dottori F., Bianchi A., Alfieri, L., Skoien, J., Salamon P.,

668 2020. River flood hazard maps for Europe and the Mediterranean Basin region. JRC Data

669 Catalogue, accessibile at http://data.europa.eu/89h/1d128b6c-a4ee-4858-9e34-6210707f3c81 ,

670 doi: 10.2905/1D128B6C-A4EE-4858-9E34-6210707F3C81

671 Note that the DOI for the dataset will be available soon. The dataset comprises the following

672 eight maps, each one available as GEOTIF file:

673 • Map of permanent water bodies for Europe and the Mediterranean Basin region

674 • River network in Europe and the Mediterranean Basin region

675 • River flood hazard maps for Europe and the Mediterranean Basin region (return periods of

676   10, 20, 50, 100, 200 and 500 years)

677 The official flood hazard maps used for the validation exercise are freely accessible at the

678 following websites:

679 • Spain: https://www.miteco.gob.es/es/cartografia-y-sig/ide/descargas/agua/zi-lamina.aspx

680   (in Spanish)

681 • Po River Basin: https://pianoalluvioni.adbpo.it/progetto-esecutivo-delle-attivita/ (in

682   Italian)

683   • Norway: https://www.nve.no/flaum-og-skred/kartlegging/flaum/ (in Norwegian)

684   • England: https://data.gov.uk/dataset/bed63fc1-dd26-4685-b143-2941088923b3/flood-

685   map-for-planning-rivers-and-sea-flood-zone-3 ; https://data.gov.uk/dataset/cf494c44-

686   05cd-4060-a029-35937970c9c6/flood-map-for-planning-rivers-and-sea-flood-zone-2

687   • Hungary: https://www.vizugy.hu/index.php?module=content&programelemid=62 (in

688   Hungarian)

689 The LISFLOOD hydrological model used in this research is released as open-source software

690 and available at https://ec-jrc.github.io/lisflood/.

691 The LISFLOOD-FP hydrodynamic model used in this research can be requested to the authors

692 for research and non-commercial purposes at

693 http://www.bristol.ac.uk/geography/research/hydrology/models/lisflood/

694

Appendix A: meteorological observations used for LISFLOOD simulations

696 The long-term run of the hydrological model LISFLOOD is based on observed data from

697 meteorological stations and precipitation datasets, which are collected and continuously

698 expanded as part of the development work for EFAS. The meteorological variables considered

699 are: precipitation, minimum and maximum temperature, wind speed, solar radiation and vapour

700 pressure. The number of stations with available meteorological observations depends on the

701 period and variable considered, with an increasing availability towards the end of the historical

702 simulation period. As an example, for the year 2016 the number of daily observations available

703 ranged from ~8.800 for temperature to ~5.500 for precipitation and ~3.700 for vapour pressure.

704 The input from meteorological stations is completed by a number of precipitation datasets

705 (EURO4M-APG, INCA-Analysis Austria, ERA-Interim GPCP corrected and Carpat-Clim; for

706 details see Arnal et al., 2019). Note that the same datasets are used to drive the LISFLOOD

707 calibration and to calculate the initial conditions for the EFAS forecasts. The data from

708 meteorological stations and gridded datasets were then interpolated using the interpolation

709 scheme SPHEREMAP to produce meteorological grids with a daily time step. The reader is

710 referred to Arnal et al. (2019) for further details.

711

Appendix B: LISFLOOD calibration results

We report here the results of the LISFLOOD calibration presented by Arnal et al. (2019). The hydrological skill of LISFLOOD is expressed by the Kling-Gupta Efficiency (KGE, Gupta et al., 2009). Figure B1 shows the spatial distribution of the hydrological skill across the EFAS domain. 75 % of all stations (543 out of 717) scored a KGE higher than 0.5 during calibration, and 57 % (409 out of 698) during validation.

It is clearly noticeable that the skill is not homogeneously distributed across Europe, with higher skills in large parts of Central Europe, and lower skill mostly in Spain caused by the strong influence of reservoirs. The other study areas considered in the validation exercise (England, Hungary, Norway, Po river basin) exhibit KGE values generally above 0.5.

Appendix C: Additional results

C1: validation results for the Po River Basin

According to Table 3, the modelled flood maps provide a better reproduction of reference maps for the Po River, compared to other study areas. False alarms are low, while hit ratio (HR) values indicate that two out of every three pixels in the reference map are correctly identified as flooded. The analysis of reference and modelled maps (Figure C1), suggests that the underestimation is partly caused by flooded areas along some tributaries which are not included in modelled maps. Other areas with omission errors are located near confluences of the Po main stem and the major tributaries in Emilia-Romagna, which may depend on the underestimation of peak flow on tributaries. In fact, the results of the LISFLOOD calibration in Figure B1 show better hydrological skill along the Po main stem, compared to some tributaries. Finally, it is likely that the inclusion of smaller tributaries of the river network in the modelled maps would improve the overall performance.
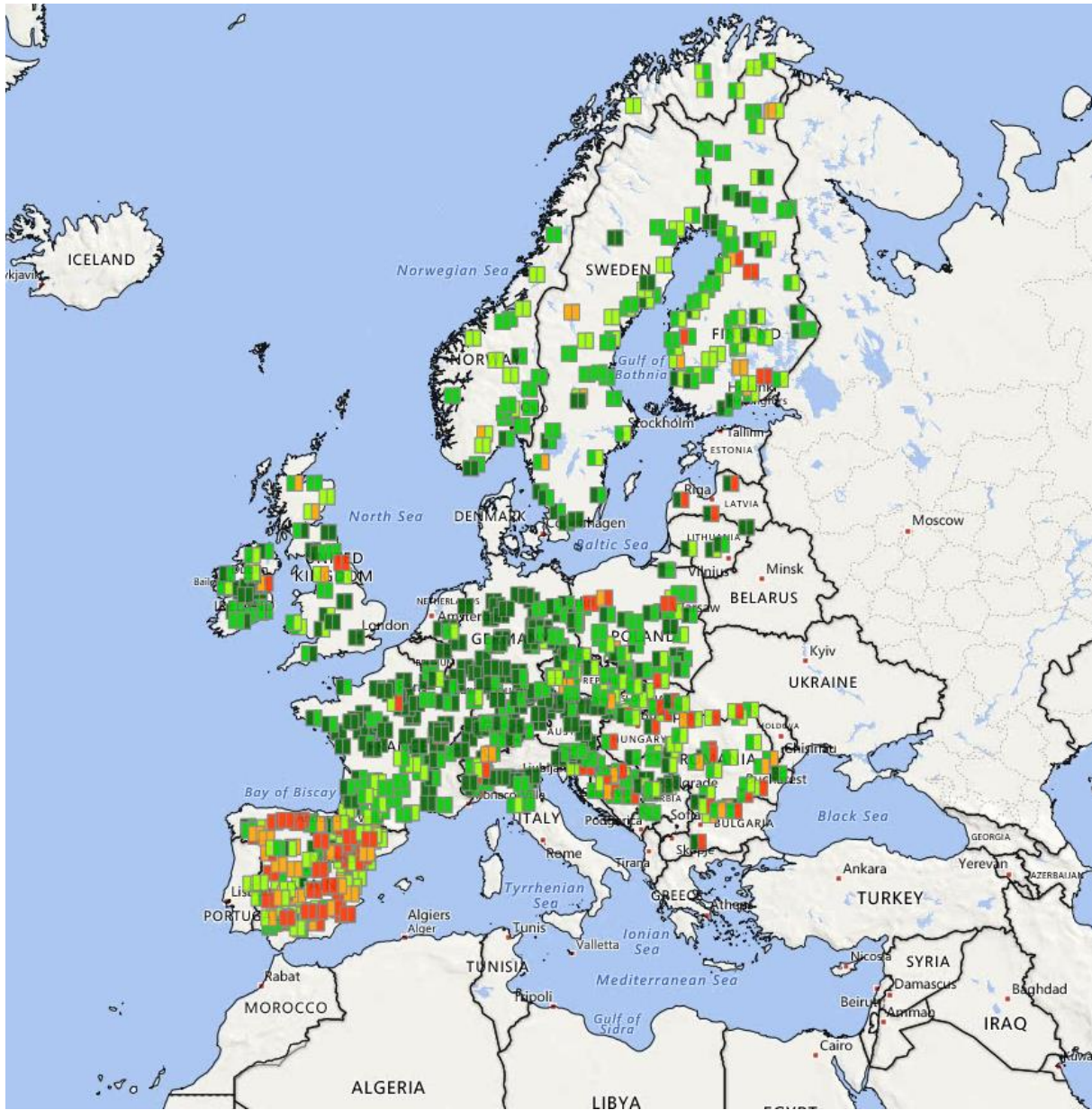
736

737 *Figure B1. Hydrological skill of EFAS at the calibration locations. Colour coding denotes the*

738 *quality of the KGE during calibration (left half of square) and validation (right half of the*

739 *square). Dark green: KGE > 0.75; Green: KGE 0.5 – 0.75, Light green: KGE 0.2 – 0.5;*

740 *Orange: 0 – 0.2; Red: < 0. Source: Arnal et al. (2019).*

741

742
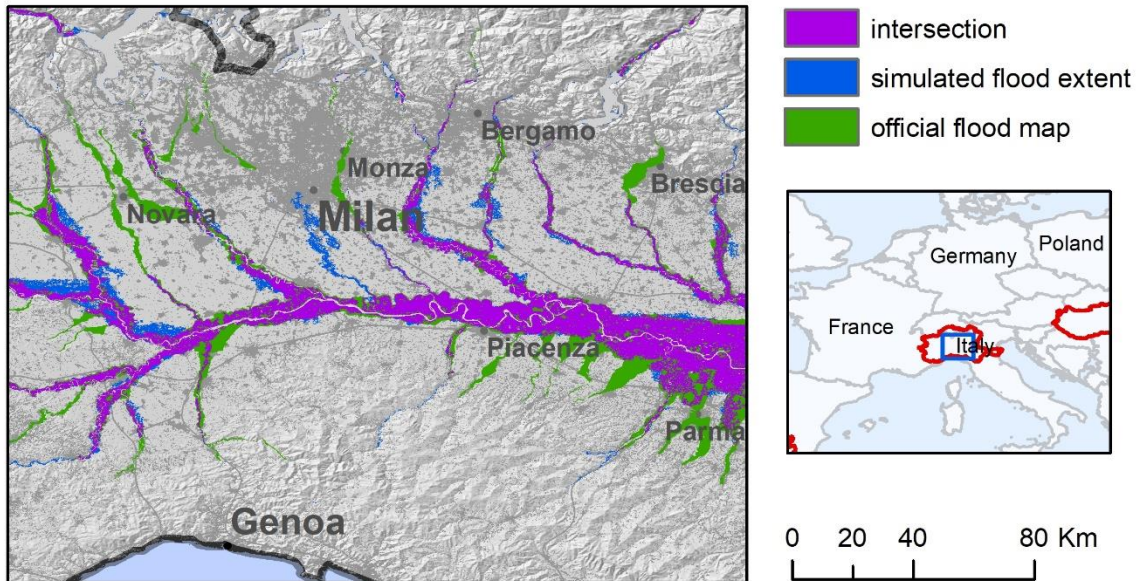
Figure C1. Comparison of modelled (blue) and reference (green) flood hazard maps (1-in-500-

year) over the Po river basin, Italy. Purple areas denotes the intersection (agreement) between

the two set of maps.

746

C2: validation results for Norway

The results of the modelled flood maps in Norway show a general tendency to overestimate flood extent for the 1-in-100-year events, with high values for both hit ratio (HR) and false alarm ratio (FAR). Such a result is in fact largely influenced by the relatively small extent and discontinuous coverage of reference maps. Flood-prone areas for the 1-in-100-year official maps only cover 215 km^2, possibly due to the low density of populated places in Norway, while they cover between 4700 and 5700 km^2 for England, Spain and Hungary. As for Spain, we applied a 5km buffer to restrict the area of comparison around reference maps, yet this leads to spurious overestimation around the edges of reference map polygons. Notably, the performance improves markedly with the use of a 1km buffer as in Wing et al., (2017), which results in increased critical success index (CSI) scores up to nearly 0.50.

The results of reported by Arnal et al. (2019) and summarized in Figure B1 suggest an acceptable hydrological skill of the LISFLOOD calibration in Norway, with a majority of gauge stations scoring KGE values above 0.5. In the areas with lower scores, the model performance for low-probability flood events might be influenced by an incorrect estimation of peak

762 discharges driven by snow melt, which plays a relevant role in determining low-probability
763 flood events.
764

C3: Influence of correcting elevation data with land use

766 We tested the results of correcting CCM DEM elevation data with vegetation cover in
767 Scandinavia, where the percentage of land covered by forests is more relevant than in the other
768 regions included in the modelled flood maps. For the 1-in100-year flood maps, the overall
769 difference in flood extent between the corrected and uncorrected maps is less than 4%, and
770 similar values were found for the other return periods. Moreover, the HR, FAR and CSI values
771 of two set of maps differ by less that 2% when calculated against the 1-in100-year official map
772 in Norway, probably because forested areas have not been considered as relevant flood-prone
773 areas. These results suggest that the simulation of densely vegetated areas have a limited
774 importance in determining the overall performance of modelled flood maps in Europe.
775

Author contribution

777

778 FD: conceptualization, formal analysis, investigation, data curation writing (original draft,
779 review and editing); LA: methodology, investigation, writing (review and editing); AB: data
780 curation, validation, visualization; JS: investigation, writing (review and editing); PS:
781 conceptualization, project administration, writing (original draft, review and editing)

782

Competing interests

784 The authors declare that they have no conflict of interest.
785

Acknowledgements

787 This study has been partially funded by the COPERNICUS programme and by an
788 administrative arrangement with Directorate General 'European Civil Protection and

789   Humanitarian Aid Operations (DG ECHO) of the European Commission. EFAS is operated and

790   financed as part of the Copernicus Emergency Management Service.

791

792

793 *References*

794   Alfieri, L., Salamon, P., Bianchi, A., Neal, J., Bates, P.D., Feyen, L., 2014. Advances in pan-
795 European flood hazard mapping, Hydrol. Process.,28 (18), 4928-4937, doi:10.1002/hyp.9947.

796   Alfieri L., Feyen L., Dottori F., Bianchi A., 2015. Ensemble flood risk assessment in Europe
797 under high end climate scenarios. Global Environmental Change 35, 199–212.

798   Alfieri, L., L. Feyen, and G. D. Baldassarre (2016), Increasing flood risk under climate
799 change: a pan-European assessment of the benefits of four adaptation strategies, Clim. Change,
800 136(3), 507–521, doi:10.1007/s10584-016-1641-1.

801   Arnal, L., S.-S. Asp, C. Baugh, A. de Roo, J. Disperati, F. Dottori, R. Garcia, M.
802 GarciaPadilla, E. Gelati, G. Gomes, M. Kalas, B. Krzeminski, M. Latini, V. Lorini, C. Mazzetti,
803 M. Mikulickova, D. Muraro, C. Prudhomme, A. Rauthe-Schöch, K. Rehfeldt, P. Salamon, C.
804 Schweim, J.O. Skoien, P. Smith, E. Sprokkereef, V. Thiemig, F. Wetterhall, M. Ziese, 2019.
805 EFAS upgrade for the extended model domain – technical documentation, EUR 29323 EN,
806 Publications Office of the European Union, Luxembourg, 2019, ISBN 978-92- 79-92881-9, doi:
807 10.2760/806324, JRC111610.

808   Bates, P. D., De Roo, A. P. J., 2000. A simple raster-based model for flood inundation
809 simulation, J. Hydrol., 236 (1–2), 54–77.

810   Bates P.D., Horritt M.S., and Fewtrell T.J., 2010. A simple inertial formulation of the
811 shallow water equations for efficient two-dimensional flood inundation modelling. Journal of
812 Hydrology, 387, 33-45.

813   Bates, P. D., Quinn, N., Sampson, C., Smith, A., Wing, O., Sosa, J., et al. (2021). Combined
814 modeling of US fluvial, pluvial, and coastal flood hazard under current and future climates.
815 Water Resources Research, 57, e2020WR028673. https://doi.org/10.1029/2020WR028673

816   Baugh, C. A., Bates, P. D., Schumann G., Trigg, M.A., 2013. SRTM vegetation removal
817 and hydrodynamic modeling accuracy, Water Resour. Res. 49, 5276–5289,
818 doi:10.1002/wrcr.20412.

819   Barredo JI, de Roo A, Lavalle C. 2007. Flood risk mapping at European scale. Water
820 Science and Technology 56: 11–17.

821   Bontemps, S., et al., 2009. GLOBCOVER -Products description and validation report, Univ.
822 Catholique de Louvain.

823   Burek, P., Knijff van der, J., Roo de, A., 2013. LISFLOOD, Distributed Water Balance and
824   Flood Simulation Model Revised User Manual 2013. Publications Office, Luxembourg.

825   Copernicus Land Monitoring Service. Corine Land Cover. http://land.copernicus.eu/pan-
826   european/corine-land-cover (accessed on 12/2/2020).

827   Dottori, F., Alfieri, L., Salamon, P., Bianchi, A., Feyen, L., Lorini, V., 2016a: Flood hazard
828   map for Europe - 100-year return period. European Commission, Joint Research Centre (JRC)
829   [Dataset] PID: http://data.europa.eu/89h/jrc-floods-floodmapeu_rp100y-tif

830   Dottori, F., Salamon, P., Bianchi, A., Alfieri, L., Hirpa, F.A., Feyen, L., 2016b.
831   Development and evaluation of a framework for global flood hazard mapping. Advances in
832   Water Resources 94, 87–102.

833   Dottori F., Kalas M.,Salamon P., Bianchi A., Alfieri, L., Feyen L., 2017. An operational
834   procedure for rapid flood risk assessment in Europe. Nat. Hazards Earth Syst. Sci., 17, 1111-
835   1126, https://doi.org/10.5194/nhess-17-1111-2017.

836   Dottori, F., Szewczyk, W., Ciscar, J.C., Zhao, F., Alfieri, L., Hirabayashi, Y., Bianchi, A.,
837   Frieler, K., Betts, R.A., Feyen, L., 2018 Increased human and economic losses from river floods
838   with   anthropogenic   warming.   Nature   Climate   Change,   8(9),   781-786,
839   https://doi.org/10.1038/s41558-018-0257-z

840   Dottori F., Bianchi A., Alfieri, L., Skoien, J., Salamon P., 2020a. River flood hazard maps
841   for Europe and the Mediterranean Basin region. JRC Data Catalogue, accessibile at
842   https://data.jrc.ec.europa.eu/dataset/1d128b6c-a4ee-4858-9e34-6210707f3c81 .

843   Dottori F, Mentaschi L, Bianchi A, Alfieri L and Feyen L, 2020b. Adapting to rising river
844   flood risk in the EU under climate change, EUR 29955 EN, Publications Office of the European
845   Union, Luxembourg, 2020, ISBN 978-92-76-12946-2 , doi:10.2760/14505, JRC118425.

846   European Commission (EC), 2007.   Directive   2007/60/EC   of   the   European
847   Parliament and of the Council on the assessment and management of flood risks,
848   Official   Journal   of   the   European   Communities, Brussels, available at: http://eur-
849   lex.europa.eu/legal-content/EN/TXT/?uri=CELEX%3A32007L0060 (accessed on 13/5/2020).

850   ESA-Airbus, 2019. Copernicus Digital Elevation Model Validation Report, accessed on
851   14/5/2020   at   https://spacedata.copernicus.eu/documents/12833/20611/GEO1988-
852   CopernicusDEM-RP-001_ValidationReport_V1.0/9bc5d392-c5f2-4118-bd60-db9a6ea4a587

853   Feyen L, Dankers R, Bódis K, Salamon P, Barredo JI. 2012. Fluvial floodrisk in Europe in

854   present and future climates. Climatic Change: 112(1): 47–62, doi:10.1007/s10584-011-0339-7.

855   Fleischmann A., R. Paiva, W. Collischonn, 2019. Can regional to continental river

856   hydrodynamic models be locally relevant? A cross-scale comparison. Journal of Hydrology X,

857   2019.

858   Gupta, H.V., H. Kling, K.K. Yilmaz, G.F. Martinez, 2009: Decomposition of the mean

859   squared error and NSE performance criteria: implications for improving hydrological

860   modelling. Journal of Hydrology, 377, 80-91.

861   Hirpa, F.A.; Salamon, P.; Beck, H.E.; Lorini, V.; Alfieri, L.; Zsoter, E.; Dadson, S.J. , 2018.

862   Calibration of the Global Flood Awareness System (GloFAS) using daily streamflow data. J.

863   Hydrol., 566, 595–606.

864   Jongman, B., Hochrainer-Stigler, S., Feyen, L., Aerts, J.C.J.H., Mechler, R., Botzen,

865   W.J.W., Bouwer, L.M., Pflug, G., Rojas, R., Ward, P.J., 2014. Increasing stress on disaster-risk

866   finance   due   to   large   floods.   Nat.   Clim.   Change   4,   264-268,

867   doi:http://dx.doi.org/10.1038/nclimate2124.

868   Kulp, S.A.; Strauss, B.H. CoastalDEM: A global coastal digital elevation model improved

869   from SRTM using a neural network. Remote Sens. Environ. 2018, 206, 231–239.

870   Liu, Y., Bates, P.D., Neal, J.C. and Yamazaki, D., 2019, December. Bare-earth DEM

871   Generation in Urban Areas Based on a Machine Learning Method. In AGU Fall Meeting

872   Abstracts (Vol. 2019, pp. H41N-1899).

873   Meadows, M.;Wilson, M. A Comparison of Machine Learning Approaches to Improve Free

874   Topography   Data   for   Flood   Modelling.   Remote   Sens.   2021,   13,   275.

875   https://doi.org/10.3390/rs13020275

876   Ministerio de Medio Ambiente y Medio Rural y Marino (MITECO), 2011. Guía

877   Metodologica para el desarrollo del sistema nacional de cartografia de zonas inundables.

878   Accessed on 18/5/2020 at https://www.miteco.gob.es/es/agua/temas/gestion-de-los-riesgos-de-

879   inundacion/snczi/Guia-metodologica-determinacion-zonas-inundables/default.aspx (in Spanish).

880   The Norwegian Water Resources and Energy Directorate, 2020. Flood Zone Maps.

881   Accessed   on   24/4/2020   at   https://www.nve.no/flaum-og-skred/kartlegging/flaum/   (in

882   Norwegian)

883   Paprotny, D., Morales-Nápoles, O., and Jonkman, S. N.: Efficient pan-European river flood

884   hazard modelling through a combination of statistical and physical models, Nat. Hazards Earth

885   Syst. Sci., 17, 1267-1283, https://doi.org/10.5194/nhess-17-1267-2017, 2017.

886   Sampson, C. C., Smith, A. M., Bates, P. D., Neal, J. C., Alfieri, L., & Freer, J. E. (2015). A

887   high-resolution global flood hazard model. *Water Resources Research*, *51*(9), 7358-7381.

888   Scussolini, P., Aerts, J. C. J. H., Jongman, B., Bouwer L. M., Winsemius H. C., de Moel H.,

889   and Ward, P. J., 2015. FLOPROS: an evolving global database of flood protection standards.

890   Nat. Hazards Earth Syst. Sci. Discuss., 3, 7275–7309, 2015, doi:10.5194/nhessd-3-7275-2015.

891   Shaw, J., Kesserwani, G., Neal, J., Bates, P., and Sharifian, M. K.: LISFLOOD-FP 8.0: the

892   new discontinuous Galerkin shallow-water solver for multi-core CPUs and GPUs, Geosci.

893   Model Dev., 14, 3577–3602, https://doi.org/10.5194/gmd-14-3577-2021, 2021.

894   Thielen J., Bartholmes J., Ramos M.H., and De Roo A. (2009). The European flood alert

895   system - part 1: concept and development. Hydrol. Earth Syst. Sci. 13, 125-140.

896   Trigg, M. et al., 2016. The credibility challenge for global fluvial flood risk analysis.

897   Environ. Res. Lett.11 094014

898   United Nations Office for Disaster Risk Reduction (UNISDR), 2015. Sendai Framework for

899   Disaster Risk Reduction 2015–2030 (www.unisdr.org/we/inform/publications/43291)

900   Van der Knijff, J.M., Younis, J., de Roo, A.P.J., 2010. LISFLOOD: a GIS-based

901   distributedmodel for river basin scale water balance and flood simulation. Int. J. Geogr. Inf. Sci.

902   24, 189-212.

903   Vogt et al., 2007. A pan-European river and catchment database, JRC Reference Reports,

904   doi:0.2788/35907.

905   Ward, P.J. et al., 2015. Usefulness and limitations of global flood risk models. Nature

906   Climate Change 5, 712–715.

907   Wendi, D.; Liong, S.-Y.; Sun, Y.; Doan, C.D. An innovative approach to improve SRTM

908   DEM using multispectral imagery and artificial neural network. J. Adv. Model. Earth Syst.

909   2016, 8, 691–702.

910   Wing, O. E., Bates, P. D., Sampson, C. C., Smith, A. M., Johnson, K. A., & Erickson, T. A.

911   (2017). Validation of a 30 m resolution flood hazard model of the conterminous United States.

912   Water Resources Research, 53(9), 7968-7986, doi:10.1002/2017WR020917.

913   Wing, O. E. J., Sampson, C. Bates, P. D., Quinn, N., Smith, A. M., Neal, J. C., C. (2019a).
914 A flood inundation forecast of Hurricane Harvey using a continental-scale 2D hydrodynamic
915 model. Journal of Hydrology X 4 , 100039.

916   Wing, O. E. J., Bates, P. D., Neal, J. C., Sampson, C. C., Smith, A. M., Quinn, N., et al.
917 (2019b). A New Automated Method for Improved Flood Defense Representation in Large-Scale
918 Hydraulic Models. Water Resources Research 55, 11007-11034, https://doi.org/2019WR025957

919   Yamazaki, D., Ikeshima, D., Tawatari, R., Yamaguchi, T., O'Loughlin, F., Neal, J.,
920 Sampson, C., Kanae, S., Bates, P. D. (2017). A high accuracy map of global terrain elevations.
921 Geophysical Research Letters.

922   Yamazaki, D., Ikeshima, D., Sosa, J., Bates, P. D., Allen, G. H., & Pavelsky, T. M. (2019).
923 MERIT Hydro: a high-resolution global hydrography map based on latest topography dataset.
924 Water Resources Research, 55, 5053–5073. https://doi.org/10.1029/2019WR024873

925   Zuzanna Zajac, Z:, Zambrano-Bigiarini, M., Salamon, P., Burek, P., Gentile, A., Bianchi,
926 A., 2013. Calibration of the LISFLOOD hydrological model for Europe. JRC technical report
927 JRC87717.